Mon. Not. R. Astron. Soc. **000**, 1–6 (1999) Printed 22 September 1999 (MN LATEX style file v1.4)

Time evolution of galactic warps in prolate haloes

M. Ideta,[1⋆] S. Hozumi,[2⋆] T. Tsuchiya[1⋆] and M. Takizawa[1⋆]
[1] *Department of Astronomy, Faculty of Science, Kyoto University, Kyoto 606-8502, Japan*
[2] *Faculty of Education, Shiga University, 2-5-1 Hiratsu, Otsu, Shiga 520-0862, Japan*

Accepted 1999 September 22. Received 1999 February 2

ABSTRACT
A recent observation with the *Hipparcos* satellite and some numerical simulations imply that the interaction between an oblate halo and a disc is inappropriate for the persistence of galactic warps. Then, we have compared the time evolution of galactic warps in a prolate halo with that in an oblate halo. The haloes were approximated as fixed potentials, while the discs were represented by N-body particles. We have found that the warping in the oblate halo continues to wind up, and finally disappears. On the other hand, for the prolate halo model, the precession rate of the outer disc increases when the precession of the outer disc recedes from that of the inner disc, and vice versa. Consequently, the warping in the prolate halo persisted to the end of the simulation by retaining the alignment of the line of nodes of the warped disc. Therefore, our results suggest that prolate haloes could sustain galactic warps. The physical mechanism of the persistence of warp is discussed on the basis of the torque between a halo and a disc and that between the inner and outer regions of the disc.

Key words: galaxies: haloes – galaxies: kinematics and dynamics – galaxies: structure – methods: numerical

1 INTRODUCTION

Many spiral galaxies, including our Galaxy, have warped discs which resemble characteristic 'cosmic integral signs'. That is, the outer disc lies above the inner disc plane on one side, and falls bellow that plane on the other side. Although the warping is often seen in neutral hydrogen layers (Sancisi 1976; Bosma 1981), it is also observed in stellar discs (van der Kruit & Searle 1981; Innanen et al. 1982; Sasaki 1987). In the Milky Way, the stellar warp has been detected not only for young stars (Miyamoto, Yoshizawa & Suzuki 1988) but for old stars (Porcel, Battaner & Jiménez-Vicente 1997). In addition, the frequency of warped discs in spiral galaxies is sufficiently large that at least half of spirals are warped both in H I discs (Bosma 1991) and in optical discs (Sánchez-Saavedra, Battaner & Florido 1990; Reshetnikov & Combes 1998). These observations imply that warps must persist for a long time unless they are repeatedly excited. It is true that some galaxies with warped discs (e.g., M31, see Innanen et al. 1982) have nearby companions. However, there do exist warped galaxies (e.g., NGC 4565, see Sancisi 1976) that have no nearby companions being supposed to be responsible for the warp in the recent past. In fact, Reshetnikov & Combes (1998) have revealed that about 21 out of 133 isolated galaxies are warped like an integral sign. This indicates that warps are not necessarily caused by tidal interactions with other galaxies.

One explanation for isolated warped galaxies is the gravitational torque of a halo acting on a disc that is 'misaligned' to the equatorial plane of the halo. Such a tilted disc embedded in a halo has intrinsic spin, so that it precesses like a top. Since the precessing rate is a function of radius, kinematical warps will wind up and disperse in a short period of time. Once the self-gravity of the disc is taken into account, realistic warped configurations emerge in which a disc precesses coherently like a solid body inside axisymmetric haloes (Sparke 1984; Sparke & Casertano 1988, hereafter SC; Kuijken 1991). Even if a tilted disc is formed in a halo as a different shape from a warped mode, it will be finally turned into the mode within a Hubble time (Hofner & Sparke 1994). However, according to some numerical simulations (Dubinski & Kuijken 1995; Binney, Jiang & Dutta 1998), the warping in oblate haloes is not retained persistently, and so, disappears within a few dynamical times. Thus, the interaction between an oblate halo and a disc will be inappropriate for long-lasting warps.

Recently, Smart et al. (1998) have extracted warp-induced motions in the Milky Way by analysing the data obtained with the *Hipparcos* satellite. Then, they have found that the Galactic warp rotates in the same direction as the Galaxy. As shown by Nelson & Tremaine (1995), oblate haloes lead to the opposite sense of the warp precession to

⋆ E-mail: ideta@kusastro.kyoto-u.ac.jp (MI); hozumi@sue.shiga-u.ac.jp (SH); tsuchiya@kusastro.kyoto-u.ac.jp (TT); takizawa@kusastro.kyoto-u.ac.jp (MT)

© 1999 RAS

the Galactic rotation, whereas prolate haloes make them rotate in accordance with each other. In addition, they have demonstrated that in some cases, prolate haloes can excite warps. Thus, prolate haloes are favourable to the explanation of Smart et al.'s (1998) finding, if the motions that they found are attributed to the interaction of the Galactic disc with an often assumed massive halo. Cosmological simulations, based on a cold dark matter scenario, have also revealed that dark matter haloes surrounding individual galaxies are highly triaxial and that the fraction of prolate haloes is roughly equal to that of oblate haloes (Dubinski & Carlberg 1991). In spite of these circumstances mentioned above, prolate haloes have somehow often been ignored in previous studies on warps. Therefore, we need to pay attention to the warp arising from prolate haloes.

In this paper, we examine how a warp is developed and evolves in prolate haloes in comparison with that in oblate haloes. As a first step, we treat the haloes as external fixed potentials. In Section 2, we describe the models and the numerical method. Results are presented in Section 3. In Section 4, we analyse our results and explain them on the basis of a simplified model. Conclusions are given in Section 5.

2 MODELS AND METHOD

We study the evolution of self-gravitating discs embedded in axisymmetric haloes. As shown by Nelson & Tremaine (1995) and by Dubinski & Kuijken (1995), dynamical friction between a disc and a halo plays an important role to precessing bending modes at least for the inner region of the composite system. However, the accurate evaluation of dynamical friction would require a prohibitively huge number of particles to represent the halo as well as the disc. Otherwise, the disc will thicken owning to two-body relaxation originating from Poisson fluctuations. In fact, Dubinski & Kuijken (1995) reported the vertical disc thickening for a self-consistent model with a particle disc, bulge, and halo. As a result, warped structures developed in the disc could not be distinguished from the background particle distribution, which would lead us to an incorrect conclusion about the longevity of the warp. Then, we begin with rigid halo models, as a first step, to unravel the effects of the halo shape on the warp.

The density distribution of the halo is an axisymmetric modification of Hernquist's models (Hernquist 1990) being suitable for spherical galaxies and bulges. Then, the halo density profile is represented, in cylindrical coordinates, by

$$\rho_{\rm h}\left(R,z\right)=\frac{M_{\rm h}}{2\pi a^2 c}\frac{1}{m\left(1+m\right)^3}, \tag{1}$$

where $M_{\rm h}$ is the halo mass, a and c are the radial and vertical core radii, respectively, and

$$m^2=\frac{R^2}{a^2}+\frac{z^2}{c^2}. \tag{2}$$

The cumulative mass profile and potential of the halo are written, respectively, by (Binney & Tremaine 1987),

$$M_{\rm h}\left(R,z\right)=M_{\rm h}\frac{m^2}{\left(1+m\right)^2}, \tag{3}$$

and

$$\Phi_{\rm h}\left(R,z\right)=-\frac{GM_{\rm h}}{2}\int_0^\infty\frac{du}{\left(a^2+u\right)\sqrt{c^2+u}\left[1+m\left(u\right)\right]^2}, \tag{4}$$

where

$$m^2\left(u\right)=\frac{R^2}{a^2+u}+\frac{z^2}{c^2+u}. \tag{5}$$

As a realistic disc model, though a bulge component is not included, we adopt an exponential density profile in the radial direction (Freeman 1970) and an isothermal sheet approximation in the vertical direction (Spitzer 1942) given by

$$\rho_{\rm d}\left(R,z\right)=\frac{M_{\rm d}}{4\pi R_{\rm d}^2 z_{\rm d}}\exp\left(-\frac{R}{R_{\rm d}}\right)\mathrm{sech}^2\left(\frac{z}{z_{\rm d}}\right), \tag{6}$$

where $M_{\rm d}$ is the disc mass, $R_{\rm d}$ is the disc scale-length, and $z_{\rm d}$ is the disc scale-height. The discs are truncated radially at 15 $R_{\rm d}$ and vertically at 2 $z_{\rm d}$. Following Hernquist's (1993) approach, we approximate the velocity distribution of disc particles using moments of the collisionless Boltzmann equation; the velocities are sampled from Gaussian distributions with means and dispersions derived from the Jeans equations. The Toomre Q parameter (Toomre 1964) used to normalize the radial velocity dispersion is set to be 1.5 at the solar radius, $\mathrm{R}_\odot = (8.5/3.5)\ R_{\rm d}$. The Q profile varies with radius and has a minimum at approximately $R = 2\ R_{\rm d}$, where the minimum Q value is about 1.47. To avoid complications due to an extra component such as a bar, this rather large Q distribution is chosen so that the bar instability will not occur in the disc.

We have ensured that the disc-halo system thus constructed is really in equilibrium if the disc is initially placed in the equatorial plane of the halo, because the density profile of the disc did not change significantly over several orbital times. However, the disc does not necessarily form in the equatorial plane of the halo. In fact, Katz & Gunn (1991) showed that the disc was misaligned to the symmetry plane of the halo at an angle of typically 30 degrees at its birth. Therefore, in our simulations the disc is initially tilted by 30 degrees with respect to the equatorial plane of the halo.

We employ a system of units such that the gravitational constant $G = 1$, the disc mass $M_{\rm d} = 1$, and the exponential scale-length $R_{\rm d} = 1$. The orbital period at the half-mass radius of the exponential disc, $R \simeq 1.7\ R_{\rm d}$, is 13.4 in our system of units. If these units are scaled to physical values appropriate for the Milky Way, i.e., $R_{\rm d} = 3.5$ kpc and $M_{\rm d} = 5.6 \times 10^{10}\ \mathrm{M}_\odot$, unit time and velocity are 1.31×10^7 yr and 262 km s^{-1}, respectively.

The disc is represented by 100 000 particles of equal mass. We show the parameters of our models in Table 5, and the rotation curves of each model in Fig. 1. The halo mass is determined so that the disc and halo masses within 3 $R_{\rm d}$ are equal to each other.

The simulations are run with a hierarchical tree algorithm (Barnes & Hut 1986) using the GRAPE-4, a special-purpose computer for gravitationally interacting particles (Sugimoto et al. 1990; Makino et al. 1997). We adopt an opening angle criterion, $\theta = 0.75$. Only monopole terms are included in the tree code. The equations of motion are integrated with a fixed time-step, $\Delta t = 0.1$, using a time-centred leapfrog method. The Plummer softening length is 0.04 $R_{\rm d}$, or in other words, 0.2 $z_{\rm d}$.

3 RESULTS

We stopped the simulations at $t = 400$. This time corresponds to about 30 orbital periods at the half-mass radius of the disc. No bar instability was found in the discs. In either simulation, the total energy was conserved to better than 0.2 per cent.

We measured the inclination and the longitude of ascending nodes of the disc relative to the equatorial plane of the halo by calculating the principal moments of inertia for the bound particles. In Fig. 2, we then show the evolving density profiles from an edge-on view of the discs in the precessing frame. In this frame, an observer is always on that line of nodes of the disc which is calculated for the particles within the half-mass radius of the disc, $R \simeq 1.7\ R_{\rm d}$. The precession periods of the discs in the oblate and prolate haloes evaluated with least-squares fits are $T_{\rm ob} = 266$ and $T_{\rm pr} = 306$, respectively. These values are in excellent agreement with those predicted by linear theory [see equation (21) of SC] which gives $T_{\rm ob} = 266$ and $T_{\rm pr} = 308$.

Hofner & Sparke (1995) showed that warped configurations are developed in oblate haloes. We further find from Fig. 2 that such configurations appear in the prolate halo as well as in the oblate one. In addition, Fig. 2 demonstrates that the shape of warp depends on that of halo: using the terminology in SC, the type I warp that bends upward away from the symmetric plane of the halo is developed in the oblate halo, while the type II warp that bends down toward the symmetric plane of the halo is developed in the prolate one. The warp in the oblate halo decayed and disappeared almost completely by the end of the simulation, while the warp in the prolate one persisted to the end.

To see the differential precession of the disc, we divided the distance between the centre and 5 $R_{\rm d}$ evenly into 10 annuli, and calculated the inclination and azimuthal angles of each annulus which contains at least 2 000 particles. Fig. 3 shows, on the polar diagram, the line of ascending nodes of each annulus with respect to the equatorial plane of the halo. There are two differences between the oblate and prolate halo models. One is the sense of the precession; for the oblate halo the warp rotates in the opposite direction to the disc rotation, while for the prolate one it rotates in the same direction. The other is the behaviour of the winding of the warp; for the oblate halo the warp winds up tightly with time, while for the prolate one the longitude of each annulus is kept almost aligned.

We find from Fig. 3 that the inner region of the disc, $R \lesssim 3\ R_{\rm d}$, precesses at almost a constant rate independent of radius both in the prolate and oblate haloes. Since the disc mass is equal to the halo mass within 3 $R_{\rm d}$ for our models, the self-gravity of the disc is dominant as compared to that of the halo within such radius. We thus understand that this behaviour arises from the predominance of the self-gravity of the disc over that of the halo, as shown by Lovelace (1998). On the other hand, the outer disc ($R \gtrsim 3\ R_{\rm d}$) precesses at a different rate from radius to radius.

To make clear the difference in precession at large radii between the oblate and prolate halo models, we present in Fig. 4 the time evolution of the longitude (top row) and that of the inclination angle (bottom row) with respect to the equatorial plane of the halo for the outer and inner discs which correspond to the annulus between 4.5 $R_{\rm d}$ and 5.0 $R_{\rm d}$, and to that between 1.5 $R_{\rm d}$ and 2.0 $R_{\rm d}$, respectively. Fig. 4 shows that the precession rate of the outer disc increases with decreasing inclination angle, and vice versa. For the prolate halo, at the beginning of the simulation, the inclination angle decreased, and the precession rate increased. In the subsequent evolution, the longitude of the outer disc passed through that of the inner disc as the inclination decreased. After the passage of the longitude of the outer disc, the inclination increased, and the precession rate decreased. For the oblate halo, on the other hand, the inclination increased initially, and the precession rate decreased. The difference in longitude between the inner and outer discs became larger with increasing inclination, and so, the warp wound up with time as seen in Fig. 3.

The difference in inclination angle between the inner and outer discs in the oblate halo is larger than that in the prolate one at the end of the simulation. However, for the oblate halo, the warp disappeared as seen in Fig. 2, because the azimuthal angle of the inner disc was different from that of the outer disc.

4 PHYSICAL INTERPRETATION

As found in the previous section, the prolate halo is plausible for the maintenance of galactic warps in that the winding problem is avoided. However, there remains a question as to what makes the difference in evolution of warps between the oblate and prolate halo models.

Since Lovelace (1998) has shown that the self-gravity of the disc can synchronize the precession rate in the inner region, we need to explain the different behaviour of the warp in the outer region between the oblate and prolate halo models. Then, we simplify the N-body models used in our simulations and construct a three-component system consisting of an outer disc, an inner disc, and an axisymmetric halo in order to pay special attention to the torque between the inner and outer discs in addition to that from the halo. Here, we approximate an outer disc as a ring.

4.1 Simple model

In this subsection, we solve the equation of motion for the outer ring in order to examine whether the results found in the N-body simulations can be reproduced. For this purpose, we consider the axisymmetric Binney (1981) potentials as models of the halo and the inner disc,

$$\Phi_{\rm h} = \frac{1}{2}V_{\rm c,h}^2 \ln\left(R_{\rm c,h}^2 + R^2 + \frac{z^2}{q_{\rm h}^2}\right), \tag{7}$$

$$\Phi_{\rm d} = \frac{1}{2}V_{\rm c,d}^2 \ln\left(R_{\rm c,d}^2 + R^2 + \frac{z^2}{q_{\rm d}^2}\right), \tag{8}$$

where $V_{\rm c}$ is the asymptotic circular velocity, $R_{\rm c}$ is the core radius, and q is the potential flattening with the subscripts 'h' and 'd' denoting the halo and the disc, respectively. The potentials of the halo and the inner disc are fixed. The inner disc is tilted by an angle of 30 degrees relative to the symmetric plane of the halo and given a constant precession rate that is calculated from linear theory (SC). The dynamics of the outer ring are solved on the basis of Euler's equation of motion for a rigid body (Goldstein 1980).

The radius and angular speed of the outer ring, Ω, are set to be 5.0 and 0.15, respectively. The parameters of this model are summarized in Table 5. The values of the potential flattening, $q_{\rm h}$ and $q_{\rm d}$, are adjusted to those which are evaluated from the halo and disc models at 5 $R_{\rm d}$ employed in the N-body simulations (see Table 5). We determine the values of $V_{\rm h,d}$ and $V_{\rm c,d}$ in the same manner.

Fig. 5 presents the time evolution of the longitude and inclination of the outer ring, which corresponds to Fig. 4 in the N-body simulations. We can see that the precession rate of the outer ring increases with decreasing inclination angle with respect to the equatorial plane of the halo, and vice versa. Moreover, for the prolate halo the inclination angle decreases at the beginning, while for the oblate one it increases. Thus, for the prolate halo, the precession of the outer ring can pass through that of the inner disc. After the passage, the inclination angle increases and the precession rate decreases. This means that the longitude of the inner disc and the outer ring remains almost aligned. Therefore, the behaviour of the outer ring is the same as that seen in the N-body simulations. Since we have found that the simple model can reproduce the main properties of the N-body simulations, we can rely on this model to figure out the physical mechanism of warps in the oblate and prolate haloes as described below.

4.2 The precession

The precession of the outer ring is caused by the torque due to the halo and the inner disc. We take a coordinate system in which the z-axis is along the symmetry axis of the halo, and the x-axis is along the line of nodes of the outer ring (where the outer ring intersects with the $z = 0$ plane). The xy-plane is in the inertial frame. The geometry is shown in Fig. 6.

The x-component of the torque exerted by the halo on the outer ring is given by

$$T_{{\rm h},x} = -\int_0^{2\pi} r d\phi \lambda \left(F_{{\rm h},y} z - F_{{\rm h},z} y\right) \quad \lambda \equiv \frac{m}{2\pi r}, \tag{9}$$

where λ is the line density of the outer ring, and m is the mass of the outer ring. The y- and z-components, $F_{{\rm h},y}$ and $F_{{\rm h},z}$, of the force due to the halo per unit mass are, respectively, written by

$$F_{{\rm h},y} = -\Omega_{\rm h}^2 y, \quad F_{{\rm h},z} = -\mu_{\rm h}^2 z, \tag{10}$$

where $\Omega_{\rm h}$ and $\mu_{\rm h}$ are the halo contributions of the orbital and vertical frequencies, respectively. The position vector of a point on the outer ring is

$$R = (r\cos\phi, r\cos i \sin\phi, r\sin i \sin\phi) \quad 0 \le \phi \le 2\pi, \tag{11}$$

where i is the inclination angle of the outer ring with respect to the equatorial plane of the halo. Then, on the assumption that $\Omega_{\rm h}$ and $\mu_{\rm h}$ are constant on the ring, we obtain

$$T_{{\rm h},x} = \frac{mr^2}{2}\left(\Omega_{\rm h}^2 - \mu_{\rm h}^2\right)\sin i \cos i. \tag{12}$$

The potential of an exponential disc in the outer region is approximated as [see equation (2P-5) of Binney & Tremain (1987)],

$$\Phi_{\rm d}(R,z) \simeq -\frac{GM_{\rm d}}{r}\left[1 + \frac{3R_{\rm d}^2\left(R^2 - 2z^2\right)}{2r^4}\right]. \tag{13}$$

Thus, the y- and z-components of the force due to the inner disc per unit mass are, respectively, given by

$$F_{{\rm d},y} = -\frac{GM_{\rm d}}{r^2}\frac{y}{r}\left[1 + \frac{15R_{\rm d}^2\left(R^2 - 2z^2\right)}{2r^4} - \frac{3R_{\rm d}^2}{r^2}\right], \tag{14}$$

and

$$F_{{\rm d},z} = -\frac{GM_{\rm d}}{r^2}\frac{z}{r}\left[1 + \frac{15R_{\rm d}^2\left(R^2 - 2z^2\right)}{2r^4} + \frac{6R_{\rm d}^2}{r^2}\right]. \tag{15}$$

Provided that the line of nodes with respect to the equatorial plane of the halo is aligned between the inner disc and the outer ring, the x-component of the torque exerted by the inner disc is

$$T_{{\rm d},x} = -\frac{mr^2}{2}\frac{9R_{\rm d}^2 GM_{\rm d}}{r^5}\sin\delta\cos\delta, \tag{16}$$

where δ is the inclination angle of the outer ring relative to the inner disc plane, and its sign is positive when the inclination angle of the inner disc is larger than that of the outer ring, and vice versa.

Next, the absolute value of the total angular momentum of the outer ring, L, is $mr^2\Omega$, where Ω is the orbital frequency, if the precession rate is rather smaller than the orbital frequency. The perpendicular component to the z-axis is $mr^2\Omega\sin i$. The change in L_x over an infinitesimally small time Δt is $mr^2\Omega\sin i\omega_{\rm p}\Delta t$, where $\omega_{\rm p}$ is the precession rate of the outer ring. Thus,

$$\dot{L_x} = mr^2\Omega\sin i\,\omega_{\rm p}. \tag{17}$$

This should be equal to the torque on the outer ring, so that the precession rate is derived as

$$\omega_{\rm p} = \frac{\Omega_{\rm h}^2 - \mu_{\rm h}^2}{2\Omega}\cos i - \frac{9R_{\rm d}^2 GM_{\rm d}}{2\Omega r^5}\frac{\sin\delta\cos\delta}{\sin i}. \tag{18}$$

If the warp is of the type I shape such as Fig. 7a, i is nearly equal to δ. It follows from equation (18) that the precession rate is proportional to $\cos i$. In this case, the second term of equation (18) is negative because δ is positive, and the first term is also negative because $\Omega_{\rm h} < \mu_{\rm h}$ for the oblate halo. Therefore, the precession rate increases with increasing inclination as seen in Fig. 4, and the difference in longitude between the outer ring and the inner disc becomes larger with time. If the warped disc is of the type II shape such as Fig. 7b, δ is negative. Taking into consideration $\Omega_{\rm h} > \mu_{\rm h}$ for the prolate halo, both terms in equation (18) are positive. Moreover, i will become smaller than $|\delta|$ with decreasing inclination, so that the second term of equation (18) is dominant. Therefore, the precession rate increases with decreasing inclination, and vice versa as seen in Fig. 4.

4.3 The inclination

The time evolution of the inclination is also explained simply by the torque on the outer ring. The geometry is the same as that used in the previous subsection except that the xy-plane is in the precessing frame of the outer ring.

The y-component of the torque, T_y, changes that of the angular momentum, $L_y = -mr^2\Omega\sin i$, and so, affects the

inclination angle, i. At the beginning, L_y suffers no change from the torque due to the halo because of the axisymmetric nature of the halo. If the longitude of the outer ring is the same as that of the inner disc, we obtain $T_y = 0$, and so, the inclination remains unchanged. If the longitude of the outer ring is smaller than that of the inner disc, i.e., a warp like a trailing spiral, T_y becomes positive. Hence, L_y increases, so that the inclination angle of the outer ring decreases. Since the torque on the inner disc is the opposite direction to that of the outer ring according to Newton's third law, the inclination of the inner disc increases. As a result, the type II warp is generated. Similarly, a warp like a leading spiral leads to the type I warp.

If the precession rate in the prolate halo decreases with radius, the warped configuration becomes similar to a trailing spiral because the sense of the precession is the same direction as the disc rotation. Consequently, the type II warp is produced, which leads to the situation where the inclination of the outer ring decreases, and the precession rate increases. In the subsequent evolution, the longitude of the outer ring passes through that of the inner disc. At the point, the warped configuration turns into that similar to a leading spiral, which, this time, leads to the situation where the inclination increases and the precession rate decreases. This kind of self-regulation enables the warped disc to avoid the differential precession. For the oblate halo, however, once the precession of the outer ring recedes from that of the inner disc, the difference in precession rate continues to increase, so that the warp winds up tightly.

4.4 Comparison with discrete bending modes

Our oblate halo model cannot sustain the warped disc, though SC found that long-lived warps do exist in some halo models. This discrepancy is considered to originate from the radial extent of a disc. SC showed that a discrete mode with an eigenfrequency ω may exist only if $\Omega - \mu < \omega < \Omega + \mu$ is satisfied at the edge of the disc, where Ω and μ are the orbital and vertical frequencies, respectively. For oblate haloes, $\Omega - \mu$ and ω are negative. Since $\Omega - \mu$ tends to zero with radius, there is some radius where ω is equal to $\Omega - \mu$. Beyond such a radius, the condition of the existence of discrete modes is violated. According to SC, bending modes become continuous in frequency ω, if a warped disc embedded in an oblate halo extends beyond the radius at which $\omega = \Omega - \mu$ holds. Consequently, such continuous modes will be propagated with a group velocity and disappear (Hunter & Toomre 1969). As is found from Fig. 8a, such a resonance radius emerges at $R \simeq 4.8\ R_{\rm d}$ in our oblate halo model. This implies that there would be no discrete bending mode and that a warped configuration would be coerced to disperse. Thus, the disappearance of the warping for the oblate halo could be due to the existence of the resonance. On the other hand, in our prolate halo model, the condition of $\Omega - \mu < \omega < \Omega + \mu$ is exactly satisfied within the truncated radius, $15\ R_{\rm d}$, as shown in Fig. 8b. Therefore, a discrete mode can exist in our prolate halo model.

Our adopted disc model is nothing special in the sense that the observed light distributions of galactic discs are well-described by an exponential law, though a constant mass-to-luminosity ratio throughout the disc is assumed. Our simulations suggest that as long as a disc is not truncated abruptly, real galactic discs would not have a discrete bending mode if surrounding haloes are oblate.

5 CONCLUSIONS

In this paper, we have examined the time evolution of warped discs in the oblate and prolate haloes using N-body simulations. The haloes were represented by fixed external potentials in which self-gravitating discs were embedded. Then, we have found the warped configurations both in the oblate and prolate haloes. While the warping in the oblate halo continued to wind up with time and finally disappeared, the warping in the prolate halo survived to the end of the simulation by regulating the line of nodes of the warped disc to be straight. We have shown that this difference in winding between the oblate and prolate haloes can be attributed to the gravitational torque between the inner and outer discs.

Observationally, some galaxies show the straight line of nodes of the warp within the Holmberg radius, beyond which the warp is traced as a leading spiral (Briggs 1990). Others show that the line of nodes is delineated as a trailing spiral (Christodoulou, Tohline, Steiman-Cameron 1988; Bosma 1991). These observations appear to favour the view that we just witness the different phases of the evolving warped discs in prolate haloes, because only warped discs in prolate haloes can change the spirality of the line of nodes according to our simulations.

Putting together our simulations and the observations mentioned above, we can infer that warps are formed and maintained in prolate haloes. However, our fixed halo models are quite simplified. In particular, such models cannot include the effect of dynamical friction between the warped disc and the halo. Dubinski & Kuijken (1995) and Nelson & Tremaine (1995) have shown that dynamical friction plays an important role to precessing discs. Therefore, we will need the simulations of warped discs embedded in live haloes to determine the precise evolution of warps, though a huge number of particles will be required to incorporate the effect of dynamical friction accurately into such simulations, and to avoid disc heating due to an insufficient number of halo particles. This line of investigation is in progress (Ideta et al. in preparation).

ACKNOWLEDGMENTS

We are grateful to Prof. S. Inagaki for his critical reading of the manuscript. We thank E. Ardi and Y. Kanamori for useful discussions, and Dr. J. Makino and the anonymous referee for valuable comments on our paper. MI thanks Dr. J. Makino for giving him an opportunity to use the GRAPE-4 and providing him with a tree code available on it. MI is also indebted to A. Kawai for his technical advice on the use of the GRAPE-4. TT and MT acknowledge the financial support from the Japan Society for the Promotion of Science.

REFERENCES

Barnes J., Hut P., 1986, Nature, 324, 446
Binney J., 1981, MNRAS, 196, 455

Binney J., Tremaine S., 1987, Galactic Dynamics. Princeton Univ. Press, Princeton, NJ
Binney J., Jiang I.-G., Dutta S., 1998, MNRAS, 297, 1237
Bosma A., 1981, AJ, 86, 1791
Bosma A., 1991, in Casertano S., Sackett P.D., Briggs F.H., eds, Warped Discs and Inclined Rings around Galaxies. Cambridge Univ. Press, Cambridge, p.181
Briggs F.H., 1990, ApJ, 352, 15
Christdoulou D.M., Tohline J.E., Steiman-Cameron T.Y., 1988, AJ, 96, 1307
Dubinski J., Carlberg R.G., 1991, ApJ, 378, 496
Dubinski J., Kuijken K., 1995, ApJ, 442, 492
Freeman K.C., 1970, ApJ, 160, 811
Goldstein H., 1980, Classical Mechanics. 2nd ed. Addison-Wesley, Reading, MA
Hernquist L., 1990, ApJ, 356, 359
Hernquist L., 1993, ApJS, 86, 389
Hofner P., Sparke L.S., 1994, ApJ, 428, 466
Hunter C., Toomre A., 1969, ApJ, 155, 747
Innanen K.A., Kamper K.W., Papp K.A., van den Bergh S., 1982, ApJ, 254, 515
Katz N., Gunn J.E., 1991, ApJ, 377, 365
Kuijken K., 1991, ApJ, 376, 467
Lovelace R.V.E., 1998, A&A, 338, 819
Makino J., Taiji M., Ebisuzaki T., Sugimoto D., 1997, ApJ, 480, 432
Miyamoto M., Yoshizawa M., Suzuki S., 1988, A&A, 194, 107
Nelson R.W., Tremaine S., 1995, MNRAS, 275, 897
Porcel C., Battaner E., Jiménez-Vicente J, 1997, A&A, 322, 103
Reshetnikov V., Combes F., 1998, A&A, 337, 9
Sánchez-Saavedra M.L., Battaner E., Florido E., 1990, MNRAS, 246, 458
Sancisi R., 1976, A&A, 53, 159
Sasaki T., 1987, PASJ, 39, 849
Smart R.L., Drimmel R., Lattanzi M.G., Binney J.J., 1998, Nature, 392, 471
Sparke L.S., 1984, ApJ, 280, 117
Sparke L.S., Casertano S., 1988, MNRAS, 234, 873 (SC)
Spitzer L., 1942, ApJ, 95, 329
Sugimoto D., Chikada Y., Makino J., Ito T., Ebisuzaki T., Umemura M., 1990, Nature, 345, 33
Toomre A., 1964, ApJ, 139, 1217
van der Kruit P.C., Searle L., 1981, A&A, 95, 105

This paper has been produced using the Royal Astronomical Society/Blackwell Science LaTeX style file.

Table 1. Parameters for N-body simulations.

	$M_{\rm d}$	$R_{\rm d}$	$z_{\rm d}$	$M_{\rm h}$	a	c
OBLATE	1.0	1.0	0.2	17.8	10.0	7.5
PROLATE	1.0	1.0	0.2	17.8	7.5	10.0

Table 2. Parameters for three-component models.

	$V_{\rm c,d}$	$R_{\rm c,d}$	$q_{\rm d}$	$V_{\rm c,h}$	$R_{\rm c,h}$	$q_{\rm h}$
OBLATE	0.5	1.0	0.8	0.7	1.0	0.9
PROLATE	0.5	1.0	0.8	0.7	1.0	1.1

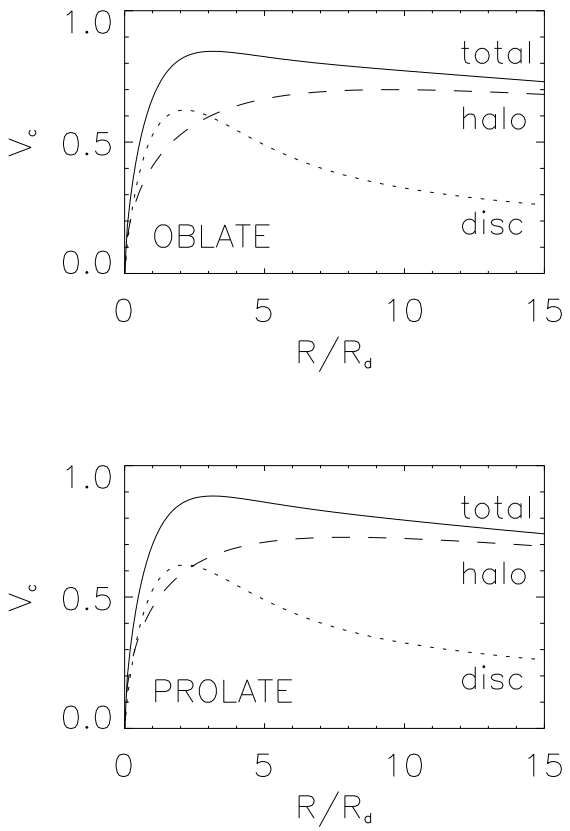

Figure 1. Circular speed showing the contribution from the disc and halo to the total for the oblate (top) and prolate (bottom) halo models.

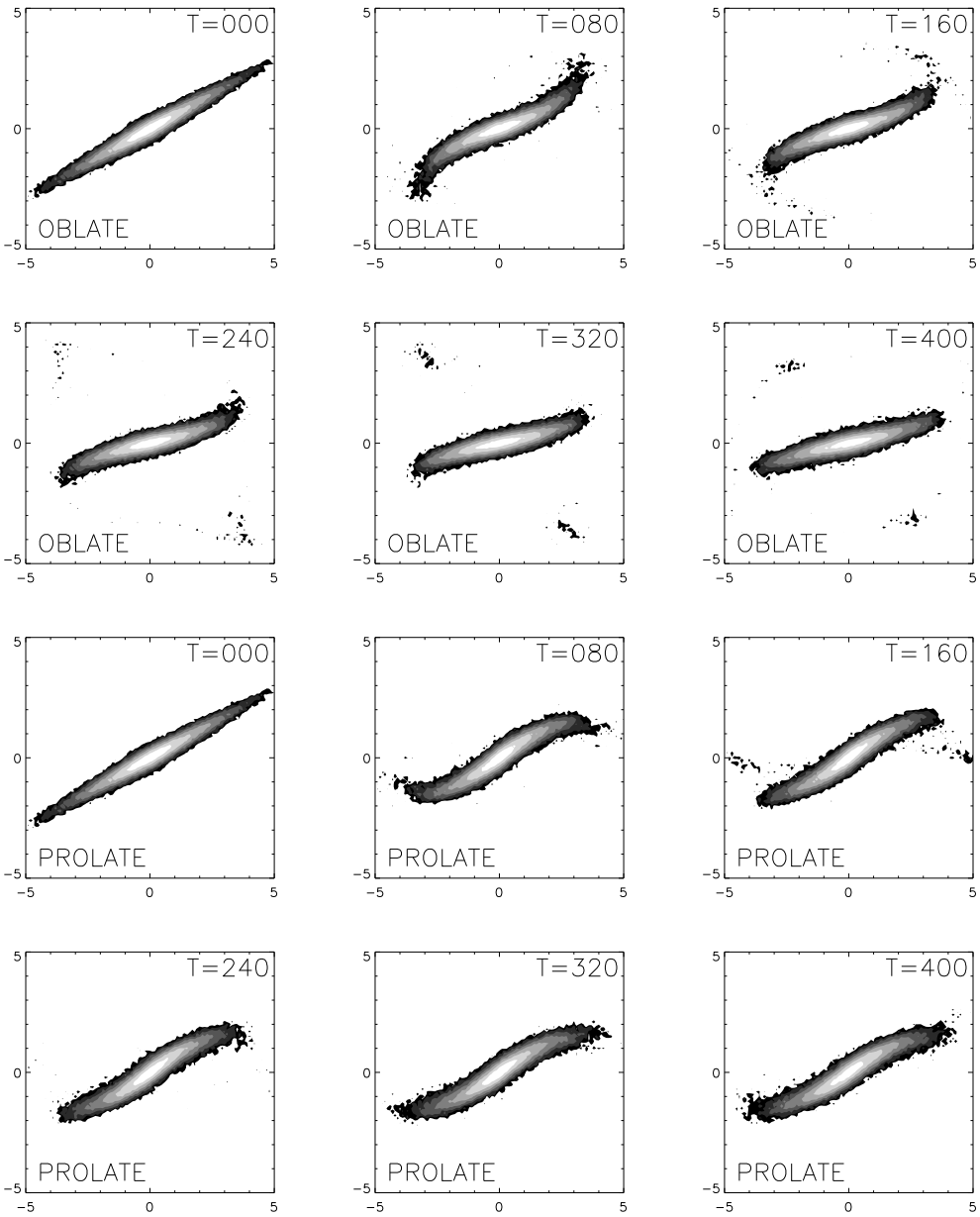

Figure 2. Time evolution of the projected density distributions of the disc in the precessing frame. The top (bottom) two rows correspond to the oblate (prolate) halo model. The time is shown at the right-up corner of each frame.

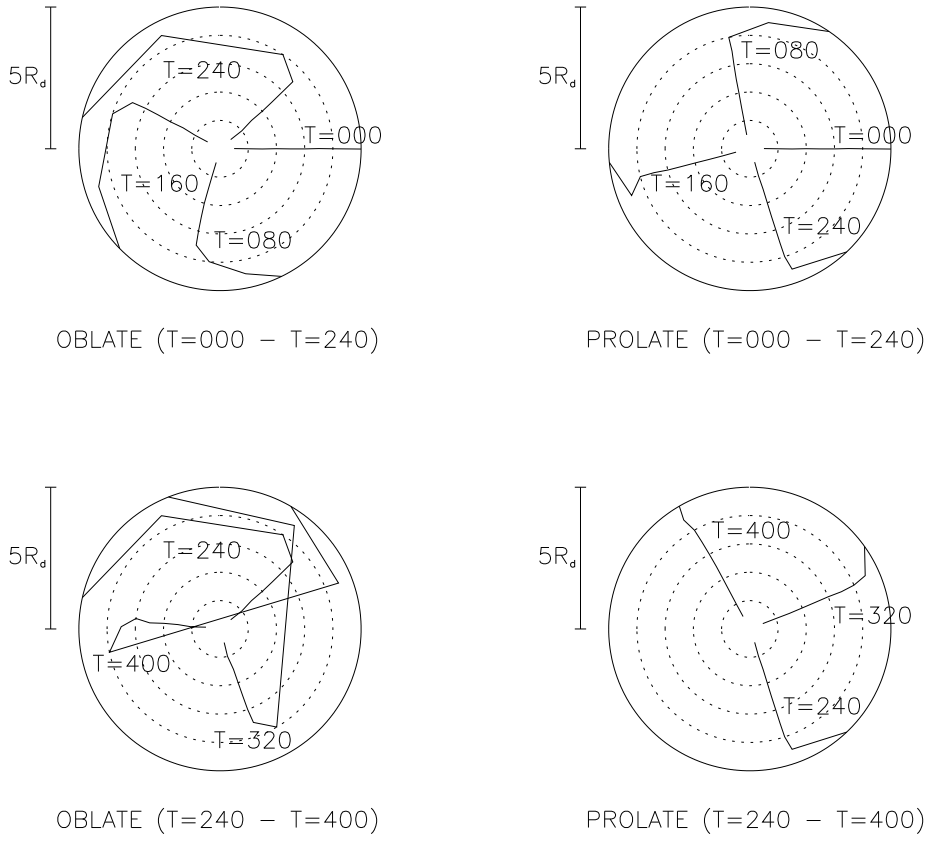

Figure 3. Time evolution of the line of ascending nodes of discs on polar diagram. The left and right columns correspond to the oblate and prolate halo models, respectively. Concentric dotted lines are drawn at a radial interval of one sale length, with a solid line at five scale lengths. The disc rotation is counterclockwise.

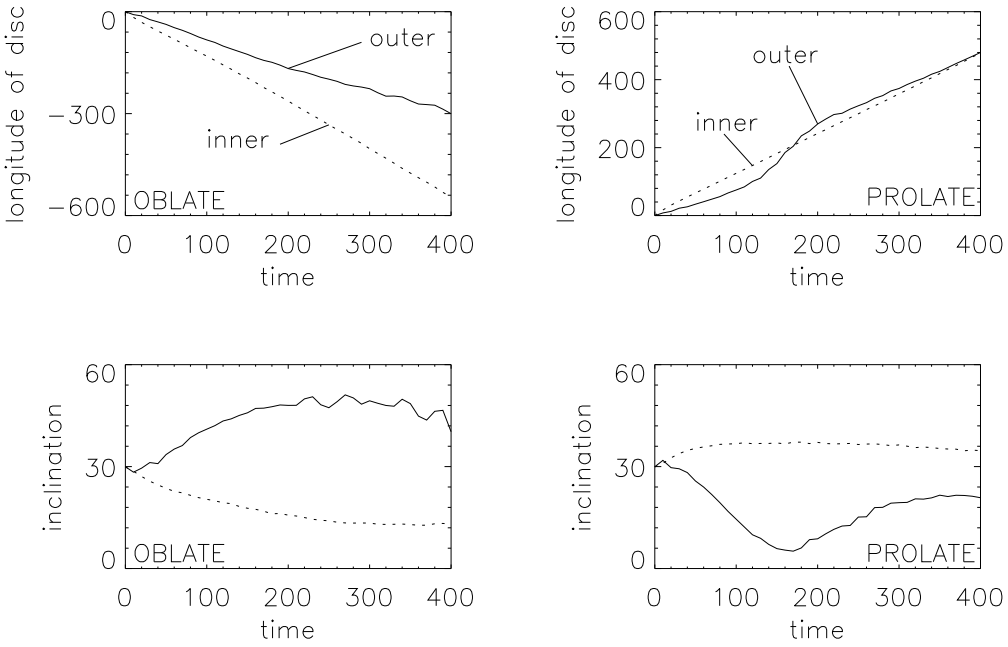

Figure 4. Time evolution of the longitude of ascending node (top row) and the inclination (bottom row) of discs. The solid and dashed lines show the outer and inner discs, respectively; the inner disc corresponds to a radial annulus between 1.5 $R_{\rm d}$ and 2 $R_{\rm d}$, and the outer disc to that between 4.5 $R_{\rm d}$ and 5 $R_{\rm d}$.

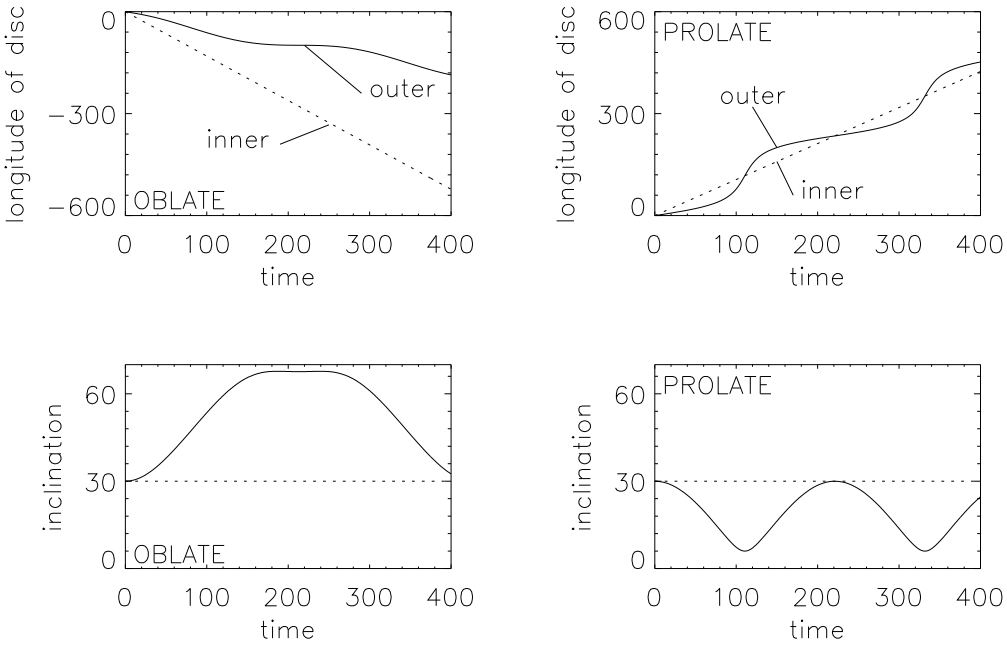

Figure 5. Same as Fig. 4, but for three-component models.

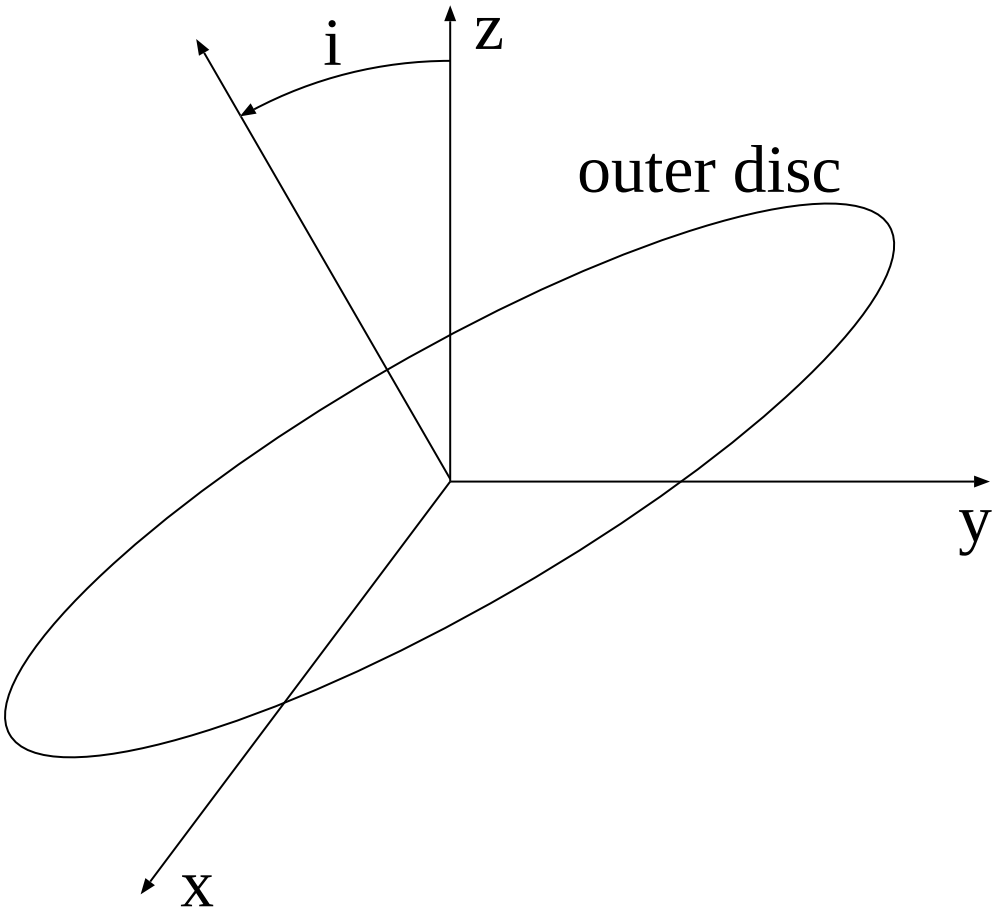

Figure 6. Geometry for the outer disc. The line of node is along the x-axis, and the symmetry axis of the halo is along the z-axis.

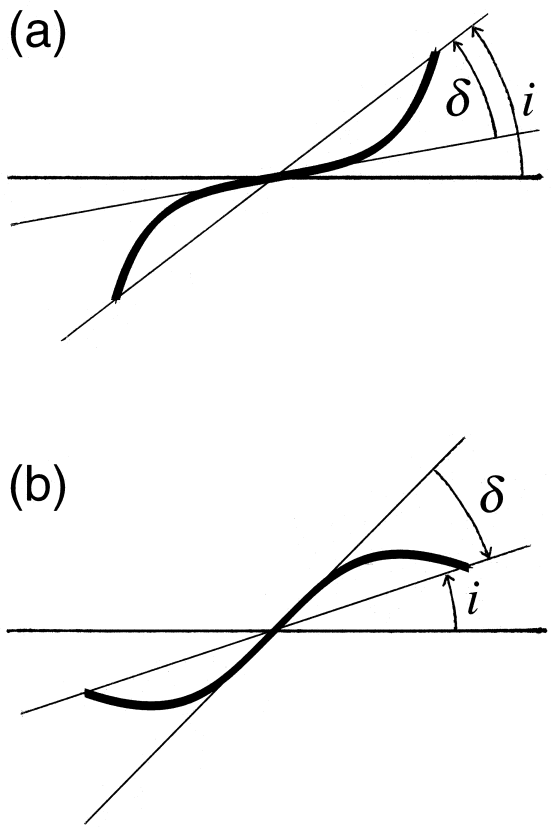

Figure 7. A sketch of the type I (a) and the type II (b) warps seen edge-on.

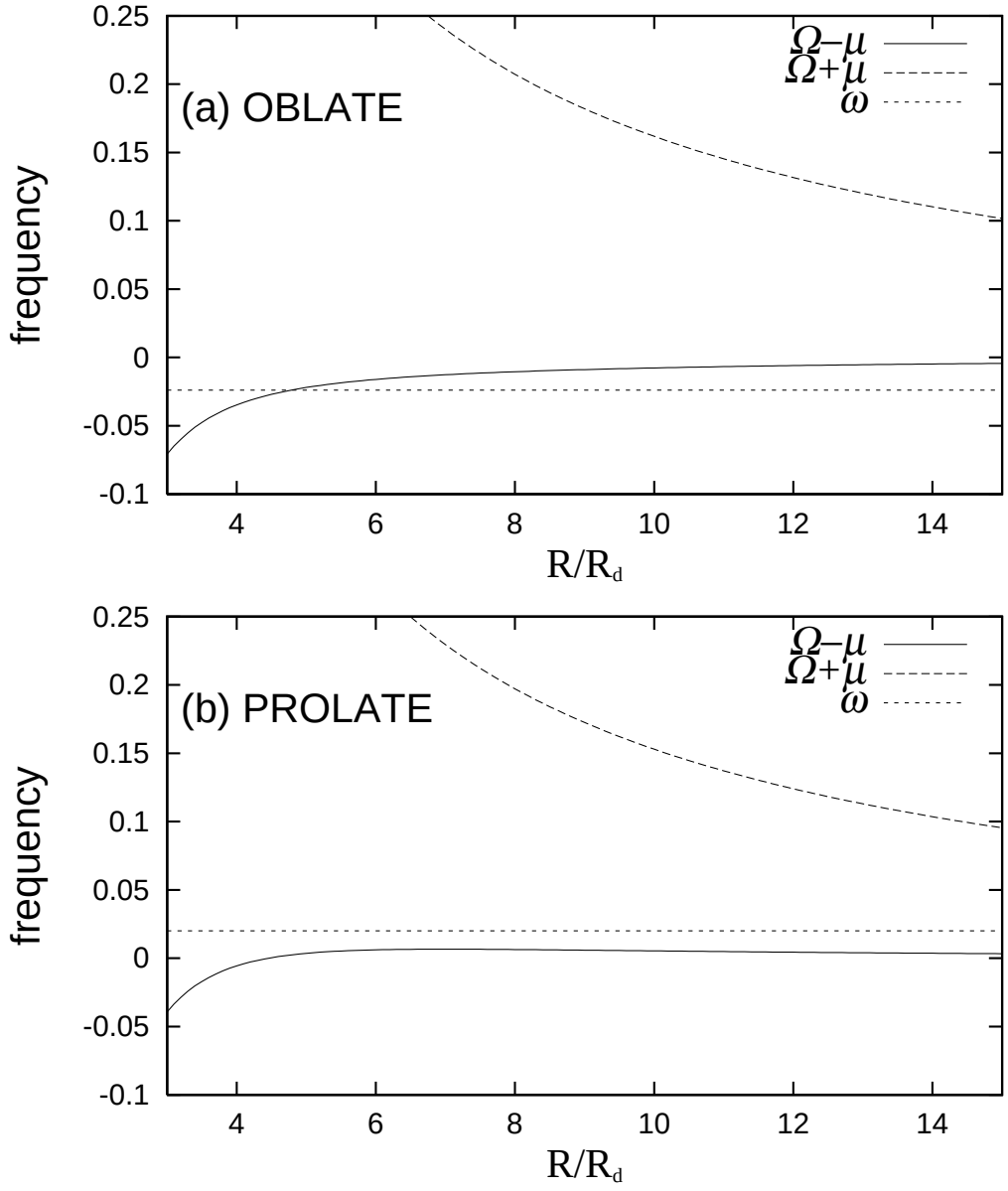

Figure 8. Plots of the frequencies, $\Omega - \mu$, $\Omega + \mu$, and ω for the oblate halo model (a) and the prolate halo model (b). In the calculation of $\Omega - \mu$ and $\Omega + \mu$, the approximated form of equation (13) is used for the disc potential.